Hindawi
Geofluids
Volume 2020, Article ID 9514691, 12 pages
https://doi.org/10.1155/2020/9514691

Research Article

Cement Grout Nonlinear Flow Behavior through the Rough-Walled Fractures: An Experimental Study

Yuhao Jin,[1,2,3] **Lijun Han**,[1,2] **Changyu Xu**,[1] **Qingbin Meng**,[2] **Zhenjun Liu**,[4] **and Yijiang Zong**[5]

[1]*School of Mechanics and Civil Engineering, China University of Mining and Technology, Xuzhou, Jiangsu 221116, China*
[2]*State Key Laboratory for Geomechanics and Deep Underground Engineering, China University of Mining and Technology, Xuzhou, Jiangsu 221116, China*
[3]*GeoEnergy Research Centre (GERC), University of Nottingham, Nottingham NG7 2RD, UK*
[4]*The Fifth Project Co., Ltd. of China Railway Bureau 14 Group, Yanzhou, Shandong 272117, China*
[5]*Jiangsu Vocational Institute of Architectural Technology, Xuzhou Jiangsu 221116, China*

Correspondence should be addressed to Lijun Han; hanlj@cumt.edu.cn

Received 31 July 2019; Revised 26 September 2019; Accepted 15 October 2019; Published 4 January 2020

Academic Editor: Zhenjiang You

This research experimentally studied the effects of various fracture roughness (characterized by the fractal dimension D) and normal stress (normal loads F_N) applied to fracture on ultrafine cement grout nonlinear flow behavior through rough-walled plexiglass fractured sample. A high-precision and effective sealing self-made apparatus was developed to perform the stress-dependent grout flow tests on the plexiglass sample containing rough-walled fracture (fracture apertures of arbitrary variation were created by high-strength springs and normal loads according to design requirements). The real-time data acquisition equipment and high-precision self-made electronic balance were developed to collect the real-time grouting pressure P and volumetric flow rate Q, respectively. At each D, the grouting pressure P ranged from 0 to 0.9 MPa, and the normal loads F_N varied from 1124.3 to 1467.8 N. The experimental results show that (i) the Forchheimer equation was fitted very well to the results of grout nonlinear flow through rough-walled fractures. Besides, both nonlinear coefficient (a) and linear coefficient (b) in Forchheimer's equation increased with increase of D and F_N, and the larger the F_N was, the larger the amplitude was. (ii) For normalized transmissivity, with the increase of Re, the decline of the $T/T_0 - \beta$ curves mainly went through three stages: viscous regime, weak inertia regime, and finally strong inertia regime. For a certain D, as the normal load F_N increased, the $T/T_0 - \beta$ curves generally shifted downward, which shows good agreement with the single-phase flow test results conducted by Zimmerman. Moreover, with the increase of D, the Forchheimer coefficient β decreased. However, within smaller F_N, β decreased gradually with increasing D and eventually approached constant values. (iii) At a given F_N, J_c increased with increasing D.

1. Introduction

Fractured rock masses (Figure 1(a)) are widely distributed in underground engineering due to geological action or excavation disturbance, which may bring serious safety hazard to the engineering stability [1–4]. Grouting is a useful way for controlling groundwater inrush and improving mechanical properties of fractured rocks in underground mining and engineering [5–9]. In order to acquire a better understanding of the grouting mechanism of fractured rock, lots of experimental studies have been performed in recent decades. For example, Sui et al. [10] experimentally carried out the study on the sealing effect of permeation grouting into specimen fractures and grout propagation patterns under water flow conditions, which obtained the influence of different factors on the sealing effect, including the initial water flow speed, fracture aperture, grout take, and gel time. Lee et al. [11] studied the reinforcement effect of cement-grouted jointed rock masses. The results showed that after grouting, the stiffnesses of the filled joints were increased up to 6 times compared with those of the ungrouted joints, meaning the mechanical properties of the jointed rock masses after

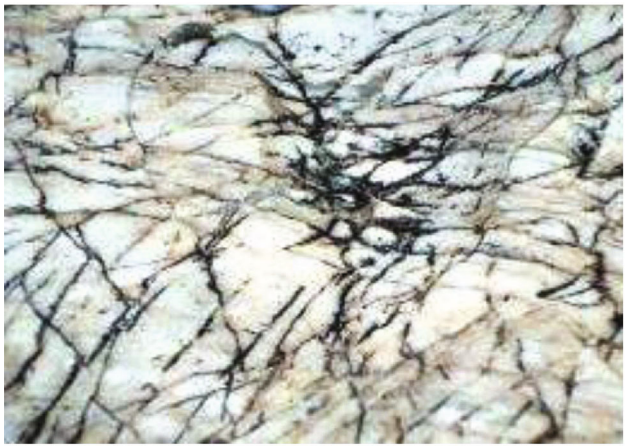

Figure 1: Fractured rock masses.

grouting were significantly improved than before. Funehag and Fransson [12] investigated a large number of experimental studies and field measurements on the penetration grouting into fractured natural rocks, which obtained the grout diffusion radius. In addition to experimental research, Kim et al. [13] conducted a series of numerical analysis by using UDEC to simulate the grout diffuse through smooth parallel surfaces based on the Bingham fluid model. They found that the grout penetration length was overestimated without considering the time-dependent hardening of grout material. Hässler et al. [14] proposed a model to simulate grout propagation in fractured rock considering time-dependent properties of the grout.

However, the previous studies on grouting mechanism mainly focused on the grouting reinforcement or seepage prevention effect for the fractured rocks after grouting (e.g., mechanical properties, sealing effect of grouted fractured rocks, and grout penetration length and diffusion radius). There were less studies on the flow behavior of cement grout through the rock fracture during the grout flow process before grout hardening. Similarly, for water, the flow behavior through rock fractures is governed by the well-known Navier-Stokes (NS) equations and the mass conservation equation written as follows [15, 16]:

$$\begin{aligned} \rho(\mathbf{u}\cdot\nabla)\mathbf{u} &= -\nabla P + \mu\nabla^2\mathbf{u}, \\ \nabla\cdot\mathbf{u} &= 0, \end{aligned} \tag{1}$$

where $\mathbf{u} = [u_1, u_2, u_3]$ stands for the velocity vector and u_1, u_2, u_3 mean the components of velocity vector; ρ, μ, and P refer to the fluid density, dynamic viscosity, and total hydraulic pressure, respectively. Nevertheless, the theory of flow through rough surface of rock fractures has not been fully developed due to the fracture roughness and fluid nonlinear flow characteristics [17]. The existence of the complex nonlinear partial differential equations and irregular rock fracture geometry makes it very difficult to solve the NS equation through real rough-walled fractures [18, 19]. For simplifying the calculation, some flow equations with assumed conditions were presented, among which the best-known equation is the cubic law that neglects the inertial terms of fluid flow through the fractures [20]. In the cubic law, the fluid flow through two smooth parallel plates was thought to be the viscous flow, and the total volumetric flow rate Q was linearly dependent on the grouting pressure gradient ∇P:

$$Q = -\frac{wb_{\mathrm{h}}^3}{12\mu}\nabla P, \tag{2}$$

where w and b_{h} are the fracture width and the hydraulic aperture, respectively. This simplified formula only applied to the laminar flow through the smooth fracture surface. However, the natural fracture is usually rough and often subjected to field stresses directly related to the fracture aperture and, hence, the fluid flow behavior through the fractures [21]. Fracture roughness has an effect on fluid flow through fractures, and the void space between opposing surfaces (fracture aperture) decreases due to the increasing normal loads [22–25]. Therefore, the characteristic of the natural rough-walled fractures under stress condition makes the actual flow rate seriously inconsistent with the results calculated using the cubic law mentioned above (equation (2)) and may cause the nonlinear flow behavior through the rough-walled rock fracture. There were many studies on the nonlinear flow in rough-walled fractures. Chen et al. [26] experimentally studied the flow through rough-walled fractures and made great contribution to the indicators representing fracture geometric characteristics. Chen et al. [27] studied the effect of geometric characteristics of deformable rough fractures under confining stresses on the non-Darcy flow behaviors. They found that the Forchheimer equation can be used to describe the non-Darcy flow in rough fractures well. Zou et al. [28] simulated the nonlinear flow in 3D rough-walled rock fractures by solving the Navier-Stokes equations and investigated the influence of shear-caused aperture changes and flow conditions (inertial term) on nonlinear flow behavior, which observed that channeling flowed along the preferential paths, transverse flowed around the contact spots, and eddy flowed behind contact spots with increasing Re. Moreover, they also studied the impacts of wall surface roughness on fluid flow through rock fractures and obtained that the high-frequency secondary roughness had a major effect on the dynamic evolution of eddy flow regions in the fracture flow field, except for the Reynolds number (Re) [29]. Li et al. [30] experimentally investigated the hydromechanical behavior of rock joints by using a parallel-plate model containing contact areas and artificial fractures. They presented some empirical relations to evaluate the influences of contact area and surface roughness on the fluid flow behavior through rock fractures. From these studies, we found that the formula accepted by most researchers for nonlinear flow through rough-walled fractures is Forchheimer's equation [31]:

$$-\nabla P = AQ^2 + BQ, \tag{3}$$

where A and B are coefficients, representing the pressure drop components caused by nonlinear and linear effects, respectively. These terms are affected by the fracture geometry and hydraulic gradient/pressure. As for the cement grout, although the grout is also a liquid before hardening, the grout flow behavior through the rock fracture is more complex than the water: due to the existence of the cement in grout, the physical properties of grout such as viscosity and density are significantly different from those of water.

In this paper, in order to study the grout flow behavior through the rough-walled fractures, a high-precision and effective sealing self-made apparatus was developed to perform stress-dependent grout flow tests on the plate specimens with fractures made of high-transparency plexiglass and high-strength springs. The plexiglass samples containing rough-walled fractures (various fracture apertures can be created by high-strength springs and normal loads) with different D (the rough morphology of the single fracture was characterized by using the fractal dimension D) were prepared. The rough morphology of the fracture was cut using a high-precision laser cutting machine. A series of tests of cement grout flow through the rough-walled fractures were performed with respect to different grouting pressures ranging from 0 to 0.9 MPa, different normal loads varying from 1124.3 to 1467.8 N, and different fracture fractal dimension D (1.1, 1.2, 1.3, 1.4, and 1.5). Based on the test results, the cement grout nonlinear flow behavior through rough-walled rock fractures with different D and normal loads was analyzed.

2. Grout Flow Testing System

A high-precision and effective sealing self-made apparatus was developed to study the stress-dependent grout flow through fractured rocks, as shown in Figures 2 and 3. This test apparatus mainly contains three parts.

2.1. A Platform for Grout Flow through Fractured Rock Sample. The platform consists of the thick bottom steel plate ($500 \times 500 \times 40$ mm) which can be used for the placement of the fractured rock sample (Figures 2(a) and 2(b)). The normal loading device ($480 \times 480 \times 20$ mm) connected to the hydraulic jack provided the normal load F_N to the fracture containing high-strength springs (Figure 2(b)). Meanwhile, the grouting pipes (5 mm in internal diameter and 9 mm in length) passing through the rectangular holes belonging to another loading device providing tangential force were inserted into the fracture and tightly sealed by using CR4305 chloroprene rubber [32–34] which ensured the sealing effect of the fracture and prevented the grout overflowing from the entrance of the fracture (Figure 4(b)). A high-strength and transparent plexiglass cover plate which was pressed under two adjustable bolt cover plates as shown in Figures 2(a) and 2(b) was placed on the fractured sample. Before each test, the plexiglass rough-walled fractured samples ($490 \times 120 \times 20$ mm in size) with different D (1.1, 1.2, 1.3, 1.4, and 1.5; see Figure 4(c)) were placed on the platform, and the horizontal and vertical loads were applied to the fractured sample boundaries.

2.2. Grout Supply and Real-Time Data and Image Acquisition System. In order to obtain the stable grouting pressure, the high-precision nitrogen regulator was installed on the nitrogen tank to achieve stable nitrogen source pressure (Figure 3(a)). Then, the stable nitrogen drove the grout to flow at a steady grouting pressure in a certain amount of time. The grouting pressure P ranged from 0-0.9 MPa which provided different grouting pressure gradient ∇P required for the tests of grout flow through fractures. The real-time data acquisition equipment consists of the high-precision pressure transmitter and paperless recorder (Figure 3(a)) which were used to collect the real-time grouting pressure P. The volumetric flow rate Q out of each fracture was derived when the quality change rates of grout flowing out of fracture were roughly the same, and the real-time grout fluid quality was obtained by the self-made high-precision electronic balance (see Figure 3(b)).

2.3. Load Supply System. The horizontal (x- and y-directions) loads on the fracture specimen were produced using adjustable hydraulic jacks (Figure 2(b)). The horizontal loading device connected to load jacks (pressure head) can apply normal uniform loads on the boundaries of the fractured sample. Moreover, the high-precision pressure sensors (Figure 2(b)) installed between the pressure head and the counterforce frames were used to feedback the values of the horizontal loads, thus guiding the adjustable hydraulic jacks to provide the fracture specimen with accurate normal boundary loads. Vertical loads applied on the specimen surface created by high-strength and transparent plexiglass cover plate were for balancing the vertical grouting pressure in the fracture and then further sealing the fractured sample.

3. Material Preparation

3.1. Grout Material. The ultrafine cement grouts (W/C ratios of 1.0 with $\rho = 1.390 \times 10^3$ (kg/m^3) and $\mu = 5.600 \times 10^{-3}$ (Pa•s)) were selected in the experiment. The ultrafine cement grouts have been widely applied in the reinforcement for underground engineering due to its more stable physical and mechanical properties, greater range of strength adjustability and better permeability, and nonpolluting nature [35]. Please note that because of the time of the grout flow through fracture in the test being very short, the grout has been in good flow state during the test. Therefore, the time-dependent hardening of grout was not considered in this paper.

3.2. Sample Material. For better conducting the visualization study of grout flow process through fracture and preset the roughness of plexiglass fractured sample which was similar to that of natural fracture, the plate fractured rock samples ($490 \times 120 \times 20$ mm in size) made of high-transparency plexiglass were prepared. Fracture morphologies are mostly irregular in actual underground engineering [36–39]. In order to simulate the irregular characteristics of fracture in nature, Ju et al. [22] presented a fractal model of single rough fracture based on the methodology. The rough morphology of

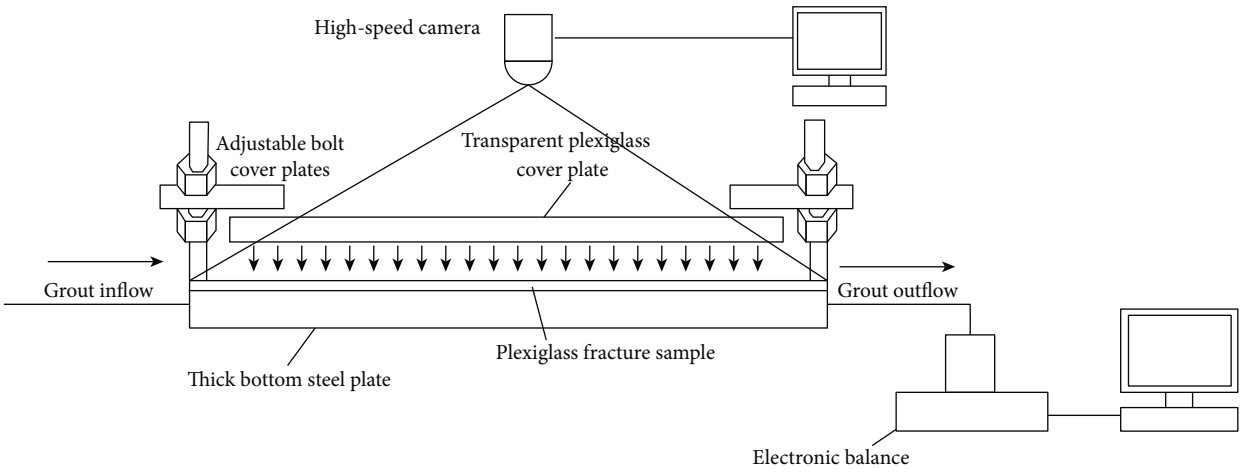

(a)

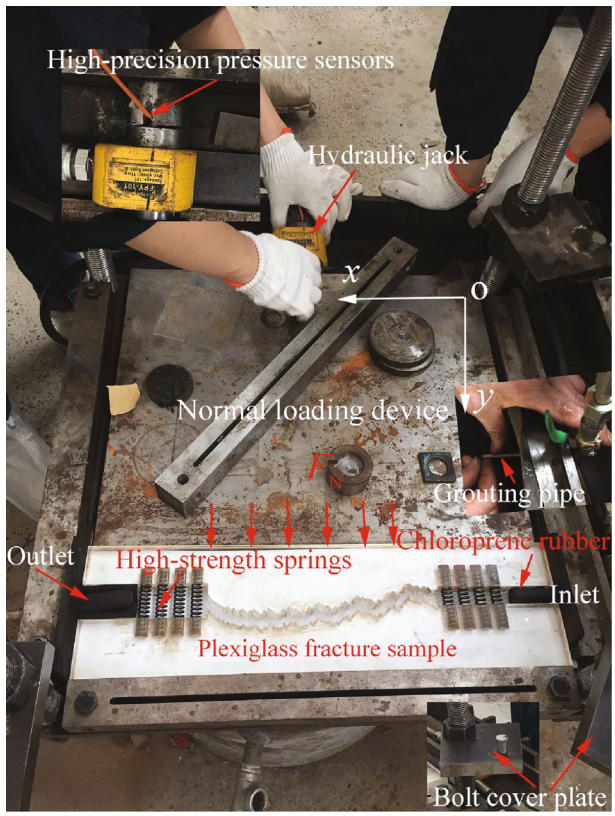

(b)

Figure 2: (a) Schematic view of grout flow testing system. (b) Actual platform for grout flow through fractured rock sample.

the single fracture was characterized by using the fractal dimension D which was based on the Weierstrass-Mandelbrot fractal function [40]

$$W(t) = \sum_{n=-\infty}^{\infty} \frac{\left(1 - e^{ib^n t}\right) e^{i\varphi_n}}{b^{(2-D)n}}, \tag{4}$$

where the parameter b is a real number larger than 1, reflecting the degree of deviation of the curve from the straight line; φ_n is an arbitrary phase angle; Fractal dimension $D \in (1, 2)$.

Using the real part of the function $W(t)$ as the fractal control function $C(t)$,

$$C(t) = \text{Re } W(t) = \sum_{n=-\infty}^{\infty} \frac{(1 - \cos b^n t)}{b^{(2-D)n}}, \tag{5}$$

where the function $C(t)$ is a fractal curve that is continuous, nondifferentiable, and D-dimensional. The fractal dimension satisfies

(a) (b)

Figure 3: (a) Grout supply system. (b) Real-time data acquisition equipment.

$$D_{HB} - \left(\frac{B}{b}\right) \leq D \leq D_{HB}, \tag{6}$$

where B represents a constant; D_{HB} represents Hausdorff-Besicovitch dimension. MATLAB was used to generate the fractal curve $C_i(t)$ with different fractal dimensions D_i on the computer, and then, the fractal fractures (rough morphologies) were cut according to the function $C_i(t)$ on the plexiglass mold by using the high-precision laser cutting machine (Figure 4(a)). $D = 1.1$, $D = 1.2$, $D = 1.3$, $D = 1.4$, and $D = 1.5$ were selected to study the effect of fracture roughness on the grout flow behavior through rough-walled fractures, and the higher the fractal dimension, the larger the fracture roughness was (Figure 4(c)). The high-strength springs that were used to simulate the variations in the fracture aperture were the important component of the fractured sample (Figure 4(b)). On the plexiglass sample, the reasonable setting of sizes of inlet (outlet) and springs ensured the uniform distribution of normal loads to the sample boundary (see Figure 4(b)).

3.3. Sealing of the Fractured Sample. For ensuring that no air or grout leakage occurred under grouting pressure condition, sealing of the fracture in the sample was the key to the success of the grouting test. The "CR4305 chloroprene rubber" was selected in this experiment after many attempts (Figure 4(b)). The CR4305 chloroprene rubber is a compressible and waterproof material that is compressed under normal loads, which seals the entrance and exit of the fracture. A piece of transparent crystal plate of a suitable size and 2 mm thickness was attached on the fractured sample, and then, the fractured sample with the transparent crystal plate was covered with a high-strength and transparent plexiglass cover plate of a suitable size and 30 mm thickness. When the fracture was preliminarily pressed tight by the transparent plexiglass cover plate, the sealed fractured sample was placed on the platform, and then, the horizontal loading device applied horizontal loads to the sample. In the grout flow testing apparatus, the transparent plexiglass cover plate provided uniform and powerful vertical loads generated by two strong bolt cover plates to further seal the fracture and balance the vertical grouting pressure in the fracture (see Figures 2(a) and 2(b)).

4. Results and Analysis

4.1. Stress-Dependent Grout Flow Behavior through Rough-Walled Fracture. From the theory of hydraulics, J is defined as the ratio of the hydraulic head difference to the flow length, calculated as follows:

$$J = \frac{(P/\rho g)}{L} = \frac{\nabla P}{\rho g}, \tag{7}$$

where J here is called grout hydraulic gradient in this paper. P is the grouting pressure obtained by the pressure transmitter and paperless recorder in real time. ρ is the grout density (1.390×103 (kg/m^3)). L is the flow length that is 0.24 m. Note that ∇P is linearly related to P at the fluid inlet: $\nabla P = P/L$. The hydraulic head at the grout outlet of the fracture was assumed to equal zero. Thus, the grouting pressure gradient ∇P ranged from 0 to 3.75 MPa/m.

From Figure 5, the relationship between J and Q showed obvious nonlinear characteristics. The linear Darcy's law can no longer be used to describe the nonlinear grout flow behavior through the rock fracture. The zero-intercept quadratic equation used to describe the nonlinear flow behavior through fractures was presented by Forchheimer in 1901 (equation (3)). This nonlinear flow model has been widely adopted by many scholars [24, 41, 42]. Combined with equation (7), equation (3) can be written to

$$J = aQ^2 + bQ, \tag{8}$$

where $a = -A\rho g$ and $b = -B\rho g$.

The relationship between the grout hydraulic gradient J and the volumetric flow rate Q of grout flow through rough-walled fracture with different D subjected to various F_N values ranging from 1124.3 to 1467.8 N was displayed in Figure 5. Referred to equation (8), the experimental data were

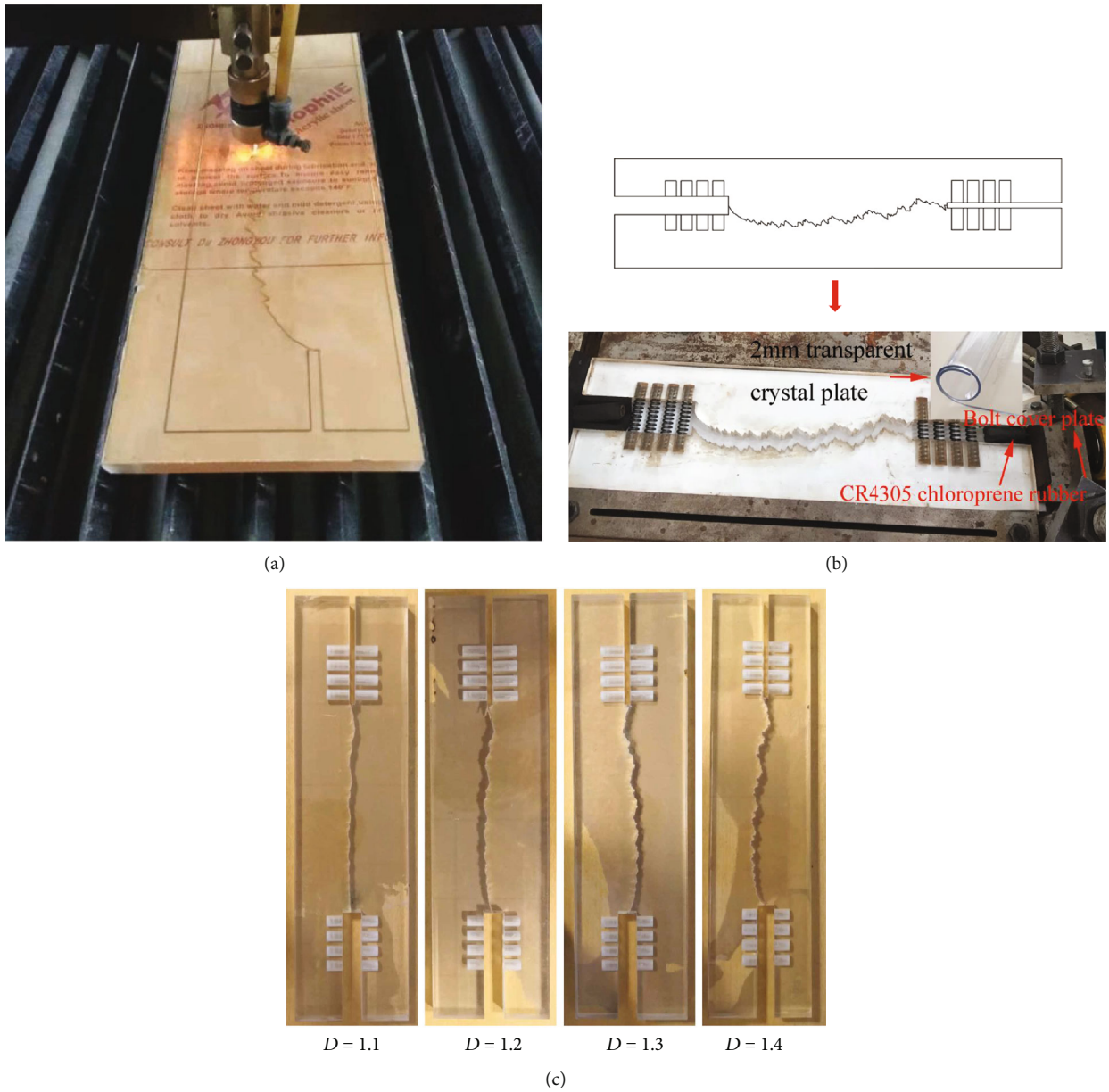

FIGURE 4: (a) High-precision laser cutting machine. (b) High-transparency plexiglass plate fractured sample of $D = 1.5$. (c) Fractured samples of different D.

well fitted and analyzed by the Forchheimer equation (Figure 5 and Table 1); the values of the correlation coefficient R^2 for all cases were larger than 0.99, as listed in Table 1, which shows that all of the experimental values almost agreed well with the fitting curves of zero-intercept quadratic equation. From Figure 5, at a given F_N, with the decrease of D, all of the maximum volumetric flow rate Q_{max} increased, meaning D has an obvious effect on the grout flow through rough-walled fracture. For example, Q_{max} was increased from 8.534×10^{-7} ($D = 1.5$) to 1.433×10^{-6} ($D = 1.1$), increasing by 0.68 times ($F_N = 1467.8$ N); 1.085×10^{-6} to 2.064×10^{-6} by 0.90 times ($F_N = 1353.3$ N); 4.306×10^{-6} to 7.286×10^{-6} by 0.69 times ($F_N = 1238.8$ N); 1.410×10^{-5} to 3.579×10^{-5} by 1.54 times ($F_N = 1124.3$ N), respectively. Meanwhile, at a given D, as F_N was increased (decreased), all of the maximum volumetric flow rate Q_{max} decreased, meaning F_N also has an obvious effect on the grout flow through rough-walled fracture. For example, as F_N ranged from 1124.3 N to 1467.8 N, the maximum volumetric flow rate Q_{max} decreased from 3.579×10^{-5} to 1.433×10^{-6}, decreasing by 95.99% ($D = 1.1$); 3.198×10^{-5} to 1.176×10^{-6} by 96.32% ($D = 1.2$); 2.050×10^{-5} to 1.056×10^{-6}, by 94.85% ($D = 1.3$); 1.628×10^{-5} to 9.601×10^{-7}, by 94.10% ($D = 1.4$); 1.410×10^{-5} to 8.534×10^{-7}, by 93.95% ($D = 1.5$).

In equation (8), the nonlinear and linear coefficients a and b were both calculated (see Table 1). From Figure 6, both a and b of all F_N increased with increasing D. Both coefficients a and b showed increasing trends with increasing F_N,

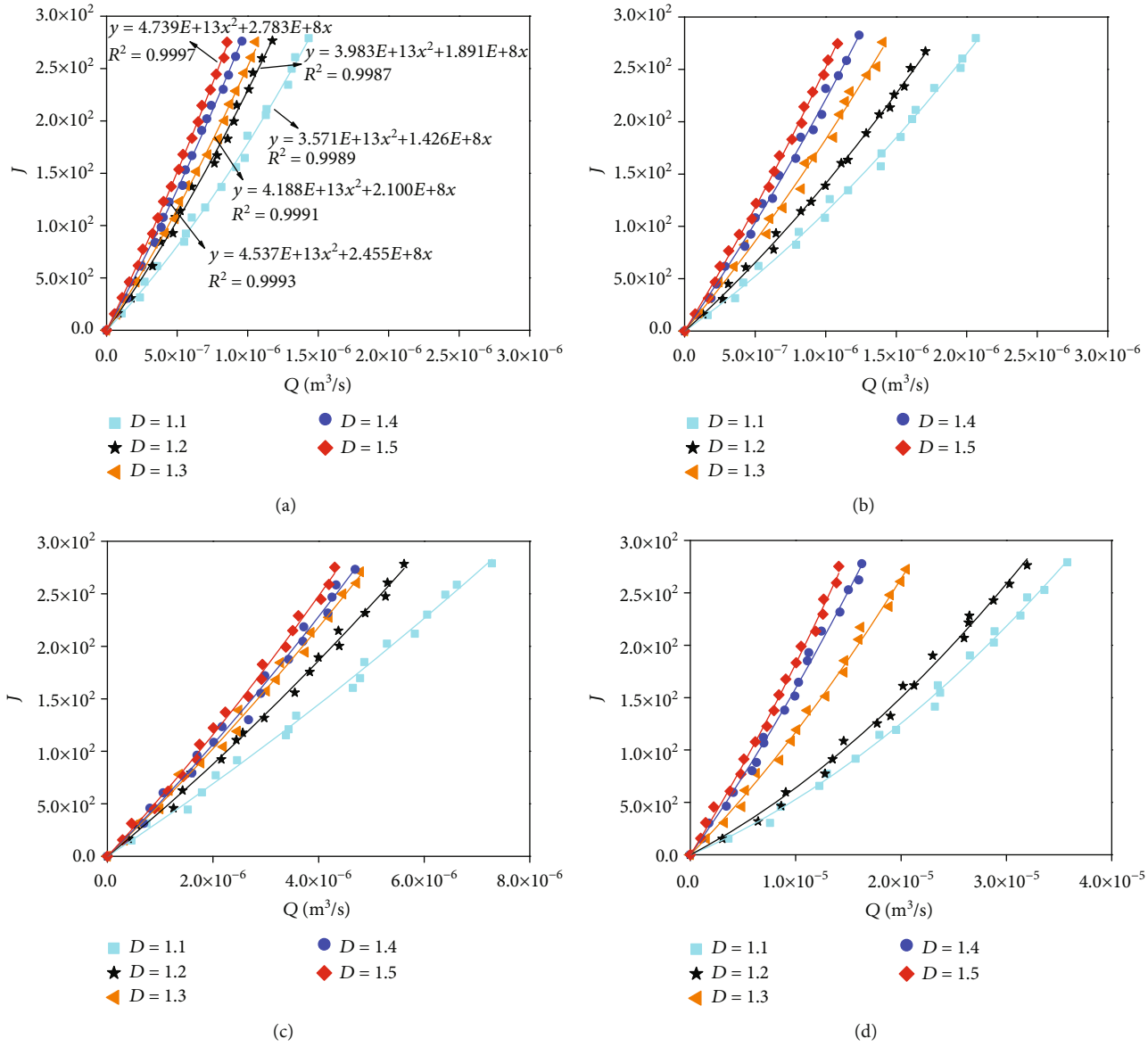

FIGURE 5: Relationships between the grout hydraulic gradient J and volumetric flow rate Q under different normal loads: (a) 1467.8, (b) 1353.3, (c) 1238.8, and (d) 1124.3 N.

and the variation trend was generally consistent with the experiments performed by Yin et al. [43]. Moreover, the larger the F_N was, the larger the amplitude was. Taking coefficients a and b for $D = 1.1$ under varying F_N as an example, a for $F_N = 1238.8$, 1353.3, and 1467.8 N was 8.131×10^{11}, 1.865×10^{13}, and 3.571×10^{13}, respectively, increasing by 7.16, 186.23, and 357.50 times over the value of 9.961×10^{10} for $F_N = 1124.3$ N. Meanwhile, b for $F_N = 1238.8$, 1353.3, and 1467.8 N was 3.289×10^7, 9.514×10^7, and 1.426×10^8, respectively, increasing by 6.68, 21.22, and 32.31 times over the value of 4.281×10^6 for $F_N = 1124.3$ N.

4.2. Normalized Transmissivity. The transmissivity T was used to estimate the nonlinear flow regimes for rock fracture samples in previous research works [44, 45]. However, T is a constant value related to the permeability and flow area of the fractured rock in Darcy's law. In this study, for grout nonlinear flow through rough-walled fractures with different D and subjected to various normal loads F_N, T was expressed as follows:

$$-\nabla P = \frac{\mu}{T} Q. \tag{9}$$

In order to evaluate the flow behavior through the rock fractures, the Reynolds number (Re) is defined as the ratio of inertial forces to viscous forces, which is typically used to quantify the onset of nonlinear flow:

$$\mathrm{Re} = \frac{\rho Q}{\mu w}. \tag{10}$$

Table 1: Measured results of a, b, R^2, and J_c for rough-walled rock fracture with different D and F_N.

W/C ratio	F_N	D	a	b	R^2	J_c
	1467.8	1.5	4.739*E*13	2.783*E*8	0.9997	209.498
		1.4	4.537*E*13	2.455*E*8	0.9993	165.246
1		1.3	4.188*E*13	2.100*E*8	0.9991	132.593
		1.2	3.983*E*13	1.891*E*8	0.9987	128.390
		1.1	3.571*E*13	1.426*E*8	0.9989	89.369
	1353.3	1.5	3.150*E*13	2.201*E*8	0.9994	204.194
		1.4	2.902*E*13	1.923*E*8	0.9988	169.805
1		1.3	2.308*E*13	1.600*E*8	0.9982	148.093
		1.2	2.055*E*13	1.204*E*8	0.9994	113.392
		1.1	1.865*E*13	9.514*E*7	0.9989	86.968
	1238.8	1.5	2.016*E*12	5.393*E*7	0.9987	205.337
		1.4	1.873*E*12	4.956*E*7	0.9983	164.345
1		1.3	1.647*E*12	4.795*E*7	0.9986	175.011
		1.2	1.352*E*12	4.117*E*7	0.9988	163.233
		1.1	8.131*E*11	3.289*E*7	0.9987	170.536
	1124.3	1.5	2.056*E*11	1.616*E*7	0.9989	163.438
		1.4	1.774*E*11	1.411*E*7	0.9986	140.736
1		1.3	1.462*E*11	1.024*E*7	0.9987	97.414
		1.2	1.114*E*11	5.273*E*6	0.9984	38.594
		1.1	9.961*E*10	4.281*E*6	0.9989	38.118

For analyzing the nonlinear flow behavior through the fracture, T_0 and T were introduced in the study [45], where the Forchheimer formula (equation (3)) was rewritten:

$$\frac{T}{T_0} = \frac{1}{1 + \beta\,\mathrm{Re}}, \tag{11}$$

where T_0 (obtained when the flow rate was sufficiently low and the inertial force was negligibly small) refers to the intrinsic transmissivity and T refers to the apparent transmissivity. β is the Forchheimer coefficient (Figure 7), which is expressed as $\beta = a\omega\mu/(b\rho)$ referred to the Forchheimer equation. Based on β, the relations between T/T_0 and Re were fitted and analyzed with different D and F_N (Figure 8). From Figure 8, for all cases, when Re was small, the viscous effect was dominant in the grout flow behavior, and T/T_0 presented a horizontal straight line (close to 1.0), the stage of which was called the viscous stage (taking Figure 8(e) as an example, Red number 1). As Re increased, the inertial effect gradually increased, and T/T_0 started to bend downward. However, during this stage, the overall grout flow behavior was still dominated by the viscous effect, and the inertial effect can be ignored, the stage of which was called the weak inertial effect stage (Figure 8(e), Red number 2). When Re increased to a certain value, T/T_0 started to decline linearly due to the strong inertial effect. At this time, the inertial effect cannot be ignored, the stage of which was called the strong inertial effect stage (Figure 8(e), Red number 3). Meanwhile, for a certain D, as the normal load F_N increased, the $T/T_0 - \beta$ curves generally shifted downward. Although there were two different fluids, this variation trend of $T/T_0 - \beta$ curves showed good agreement with the single-phase flow test results conducted by Zimmerman et al. [45]. From Figure 7, with the increase of D, most of the values of β decreased. This decreasing trend was especially evident when the normal forces were larger (e.g., F_N = 1353.3 and 1467.8 N). Taking larger F_N = 1467.8 N as an example, with the increase of D from 1.1 to 1.5, β decreased from 0.02018 to 0.01372, or by 32.01%, while β decreased gradually with the increase of D, when F_N was smaller (such as 1124.3 N). However, when F_N was 1238.8 N, as D increased, β was almost unchanged.

4.3. Critical Grout Hydraulic Gradient Analysis. The flow regime does not obey the linear Darcy's law under higher fluid flow velocity (higher pressure gradient ∇p) [27, 46, 47]. In order to further illustrate the non-Darcy flow mechanism of fluid flow through rough-walled fractures and quantify the degree of nonlinear flow effect, a factor E was proposed by Zeng and Grigg [48]:

$$E = \frac{aQ^2}{\left(aQ^2 + bQ\right)}, \tag{12}$$

where aQ^2 and bQ were energy losses due to the inertial and viscous dissipation mechanisms in the fractures, respectively. Thus, the factor E expressed the percentage of the grout hydraulic gradient drop related to the nonlinear term aQ^2 to the total grout hydraulic gradient. For grout flow through rock fractures, nonlinear flow effects may become more obvious when the volumetric flow velocity increased at the grout inlet. Previous studies have shown that in practical engineering, when the hydraulic gradient drop caused by the nonlinear flow effect was greater than 10% of the total gradient drop, the nonlinear term aQ^2 cannot be ignored [49, 50]. Therefore, the critical factor E = 0.1 was selected to evaluate the flow regime through fractures, and the corresponding J is defined as the critical hydraulic gradient J_c. The variations in J_c for all cases with different D and F_N were as shown in Figure 9 and Table 1. From Figure 9, at a given F_N, as D increased, J_c for all cases showed increasing trends, which means the fracture roughness has an important impact on the flow regime through fracture. The reason for these variations may be as follows: with the increase of D, the fracture was rougher, which would make it harder for the grout to flow through the fracture. Therefore, the grout hydraulic gradient required for grout flow entering into the nonlinear flow regime was larger. Taking F_N = 1467.8 N as an example, J_c was 128.390 (D = 1.2), 132.593 (D = 1.3), 165.246 (D = 1.4), and 209.498 (D = 1.5), respectively, increasing by 43.66%, 48.37%, 84.90%, and 134% over J_c of 89.369 for D = 1.1. Please note that, for magnitude, the magnitude of J_c in our study was not same as that in Yin et al. [43], and the difference was about an order of magnitude (J_c in our study was larger), which may be due to the viscosity of the cement grout being higher than that of water, grout entering the nonlinear flow

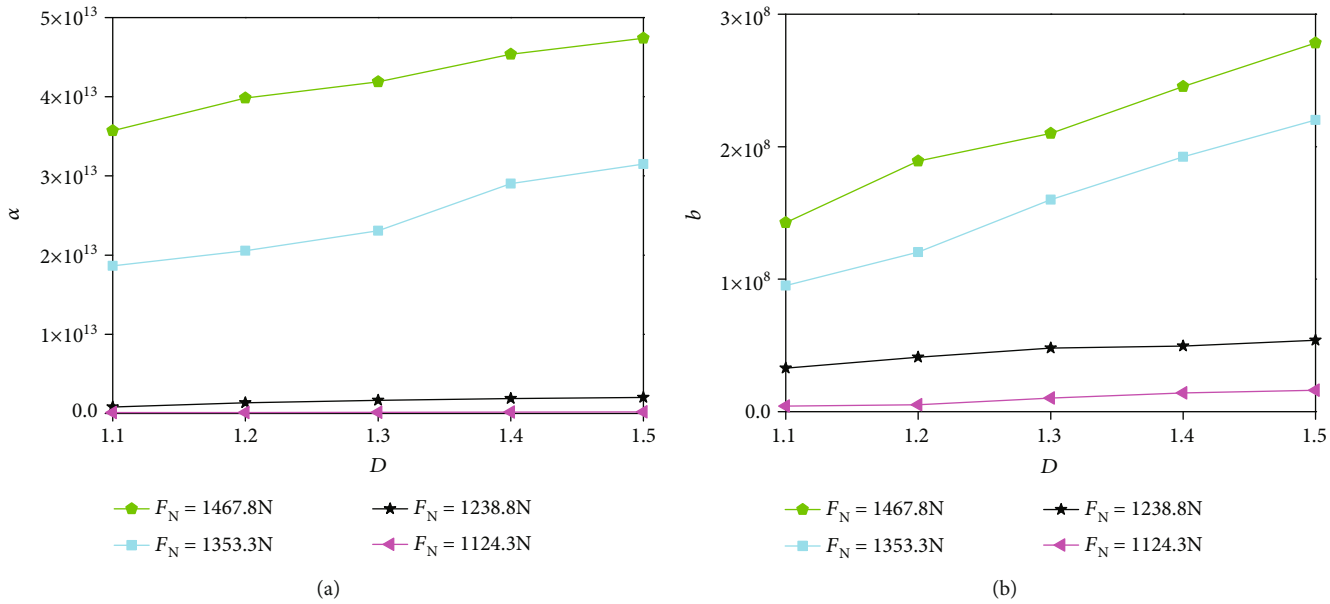

Figure 6: Variations in the (a) nonlinear coefficients a and (b) linear coefficients b.

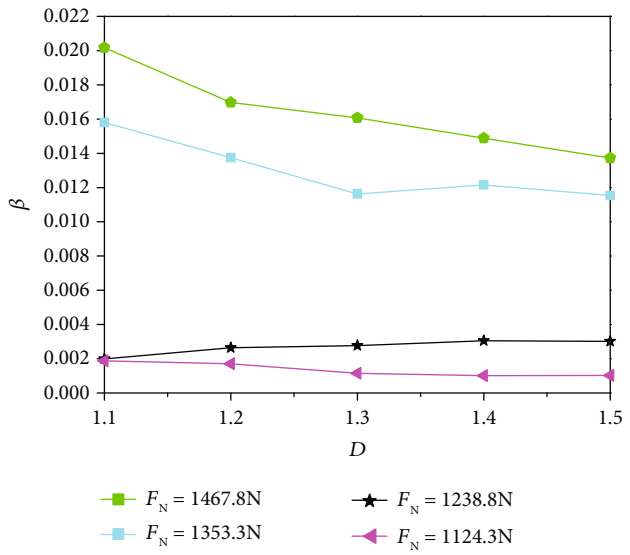

Figure 7: Variations in the Forchheimer coefficient β with increasing D.

regime required larger grout flow rate than that of water, so J_c of grout would become larger accordingly.

5. Conclusions

The effects of the fracture roughness (characterized by the fractal dimension D) and normal loads F_N on the ultrafine cement grout nonlinear flow behavior through rough-walled fracture were studied. A self-made apparatus with high precision and effective sealing characteristics was used for stress-dependent grout flow tests. The nonlinear flow behavior (J-Q), nonlinear flow regime, nonlinear and linear coefficients (a and b), normalized transmissivity ($T/T_0 - \beta$), Forchheimer coefficient (β), and critical hydraulic gradient (J_c) for grout flow through fractures were obtained. The main experimental results were as follows:

(1) The correlation between grout hydraulic gradient J and volume flow rate Q was demonstrated to be nonlinear based on the flow tests, which was fitted by the Forchheimer equation. At a given F_N, with the decrease of D, all of the maximum volumetric flow rate Q_{max} increased, meaning the fracture roughness has an obvious effect on the grout flow through rough-walled fracture. Meanwhile, at a given D, with the increase of F_N, all of the Q_{max} decreased, meaning the normal stress also has an obvious effect on the grout flow through rough-walled fracture. Moreover, both nonlinear coefficient (a) and linear coefficient (b) of all F_N increased with increasing D and F_N, and the larger the F_N was, the larger the amplitude

(2) For normalized transmissivity, when Re was small, with the increase of Re, the $T/T_0 - \beta$ curves presented a horizontal straight line (close to 1.0), the reason of which was that the viscous effect was dominant in the grout flow behavior through fracture; as Re continued to increase, $T/T_0 - \beta$ started to bend downward. During this stage, the grout flow behavior was still dominated by the viscous effect, and the inertial effect can be ignored. When Re increased to a certain value, $T/T_0 - \beta$ started to decline linearly. During this stage, the inertial effect cannot be ignored, and it became dominant in the grout flow behavior through fracture. Moreover, for a certain D, as the normal load F_N increased, the $T/T_0 - \beta$ curves generally shifted downward. The $T/T_0 - \beta$ curve variation trend showed good agreement with

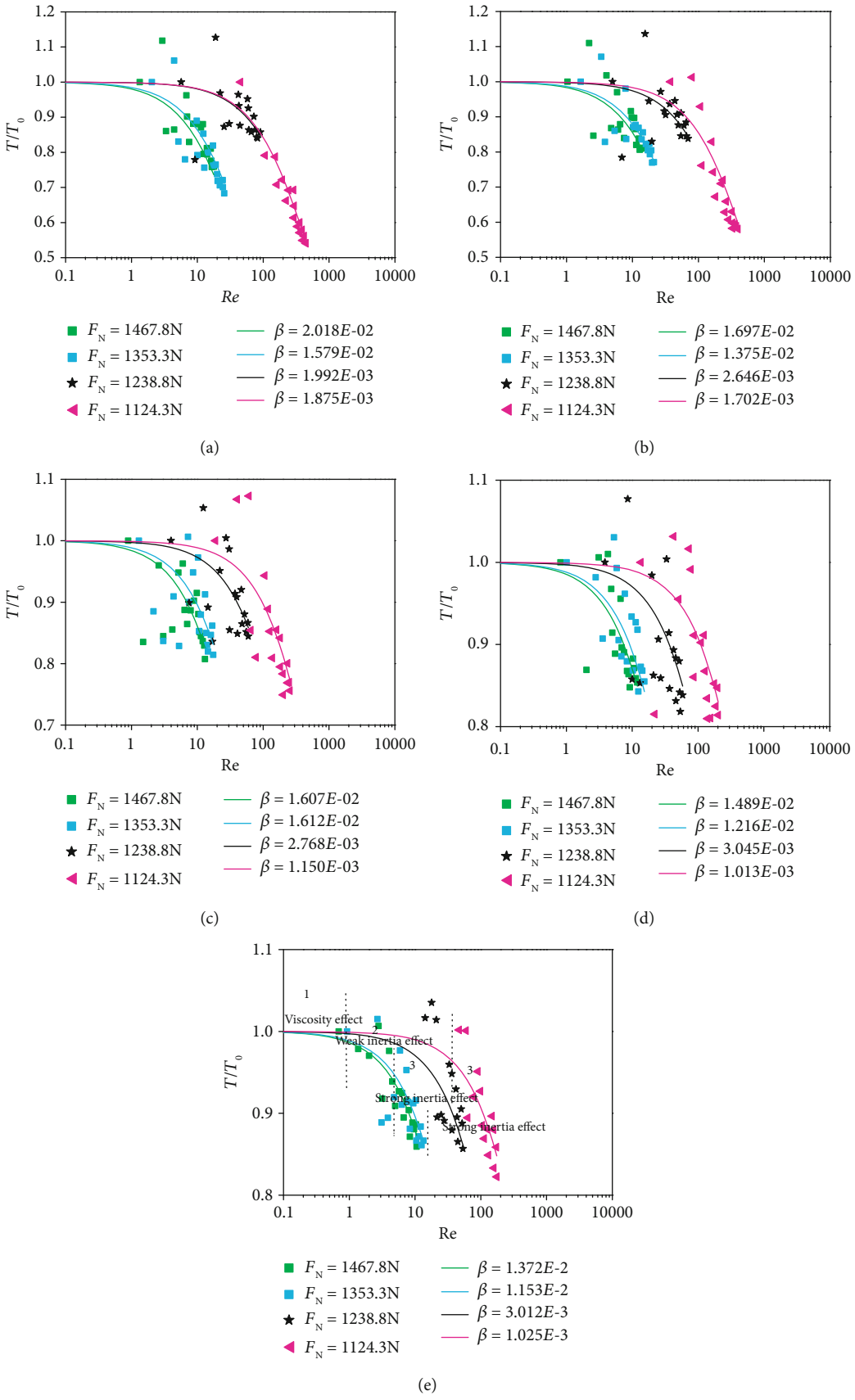

Figure 8: Relationships between the Reynolds number (Re) and the normalized transmissivity (T/T_0): (a) $D = 1.1$, (b) $D = 1.2$, (c) $D = 1.3$, (d) $D = 1.4$, and (e) $D = 1.5$.

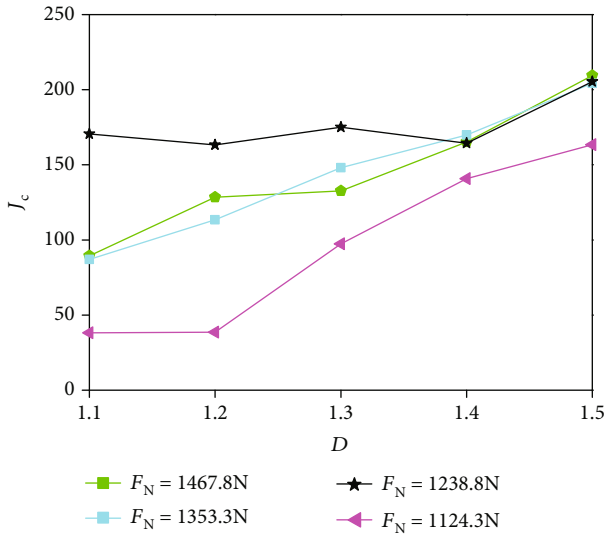

FIGURE 9: Relationships between J_c and different D under various normal loads F_N.

the single-phase flow test results conducted by Zimmerman. For the Forchheimer coefficient β, with the increase of D, β decreased. Within smaller F_N, β decreased gradually with the increase of D and eventually approached constant values

(3) At a given F_N, J_c increased with the increase of D, which means the fracture roughness has a significant effect on the flow regime through fracture. The magnitude of J_c in our study was an order larger than that in Yin et al. [43], which may be because the cement grout viscosity was higher than that of water, grout entering the nonlinear flow regime needed larger grout flow rate than that of water. Therefore, J_c of grout would be larger accordingly

In the future research, the split grouting in the deep fractured rock mass and cement grout flow behavior through 3D fractures with contacts will be the focus of our study.

Data Availability

The data used to support the findings of this study are included within the article.

Conflicts of Interest

The authors declare no conflict of interest.

Acknowledgments

This work was supported by the joint Ph.D. program of "double first rate" construction disciplines of CUMT.

References

[1] M. Chen, S. Yang, R. Pathegama Gamage et al., "Fracture processes of rock-like specimens containing nonpersistent fissures under uniaxial compression," *Energies*, vol. 12, no. 1, p. 79, 2019.

[2] Y. H. Jin, L. J. Han, Q. B. Meng, S. Sanda, H. Z. Zang, and B. Feng, "Mechanical properties of grouted crushed coal with different grain size mixtures under triaxial compression," *Advances in Civil Engineering*, vol. 2018, Article ID 9473947, 13 pages, 2018.

[3] Q. H. Lei, J. P. Latham, and C. F. Tsang, "The use of discrete fracture networks for modelling coupled geomechanical and hydrological behaviour of fractured rocks," *Computers and Geotechnics*, vol. 85, pp. 151–176, 2017.

[4] S. Q. Yang, M. Chen, H. W. Jing, K. F. Chen, and B. Meng, "A case study on large deformation failure mechanism of deep soft rock roadway in Xin'an coal mine, China," *Engineering Geology*, vol. 217, pp. 89–101, 2017.

[5] Y. H. Jin, L. J. Han, Q. B. Meng et al., "Experimental investigation of the mechanical behaviors of grouted sand with UF-OA grouts," *Processes*, vol. 6, no. 4, p. 37, 2018.

[6] D. S. Park and J. Oh, "Permeation grouting for remediation of dam cores," *Engineering Geology*, vol. 233, pp. 63–75, 2018.

[7] Q. Wang, S. Y. Wang, S. W. Sloan, D. C. Sheng, and R. Pakzad, "Experimental investigation of pressure grouting in sand," *Soils and Foundations*, vol. 56, no. 2, pp. 161–173, 2016.

[8] K. Wu, M. Y. Ma, and D. X. Hao, "Study on grouting pressure of splitting grouting based on cylindrical expansion considering large strain," *Advanced Materials Research*, vol. 378-379, pp. 288–291, 2011.

[9] G. Zheng, X. S. Zhang, Y. Diao, and H. Y. Lei, "Experimental study on grouting in underconsolidated soil to control excessive settlement," *Natural Hazards*, vol. 83, no. 3, pp. 1683–1701, 2016.

[10] W. H. Sui, J. Y. Liu, W. Hu, J. F. Qi, and K. Y. Zhan, "Experimental investigation on sealing efficiency of chemical grouting in rock fracture with flowing water," *Tunnelling and Underground Space Technology*, vol. 50, pp. 239–249, 2015.

[11] J. S. Lee, C. S. Bang, Y. J. Mok, and S. H. Joh, "Numerical and experimental analysis of penetration grouting in jointed rock masses," *International Journal of Rock Mechanics and Mining Sciences*, vol. 37, no. 7, pp. 1027–1037, 2000.

[12] J. Funehag and Å. Fransson, "Sealing narrow fractures with a newtonian fluid: model prediction for grouting verified by field study," *Tunnelling and Underground Space Technology*, vol. 21, no. 5, pp. 492–498, 2006.

[13] H. M. Kim, J. W. Lee, M. Yazdani, E. Tohidi, H. R. Nejati, and E. S. Park, "Coupled viscous fluid flow and joint deformation analysis for grout injection in a rock joint," *Rock Mechanics and Rock Engineering*, vol. 51, no. 2, pp. 627–638, 2018.

[14] L. Hässler, U. Håkansson, and H. Stille, "Computer-simulated flow of grouts in jointed rock," *Tunnelling and Underground Space Technology*, vol. 7, no. 4, pp. 441–446, 1992.

[15] D. J. Brush and N. R. Thomson, "Fluid flow in synthetic rough-walled fractures: Navier-stokes, stokes, and local cubic law simulations," *Water Resources Research*, vol. 39, no. 4, p. 1085, 2003.

[16] R. W. Zimmerman and G. S. Bodvarsson, "Hydraulic conductivity of rock fractures," *Transport in Porous Media*, vol. 23, no. 1, pp. 1–30, 1996.

[17] M. Zambrano, A. D. Pitts, A. Salama, T. Volatili, M. Giorgioni, and E. Tondi, "Analysis of fracture roughness control on permeability using sfm and fluid flow simulations: implications for carbonate reservoir characterization," *Geofluids*, vol. 2019, Article ID 4132386, 19 pages, 2019.

[18] N. Y. Ko, S. H. Ji, Y. K. Koh, and M. H. Baik, "Hydraulic conceptualization of a single fracture using hydraulic interference tests at a deep underground condition," *Geosciences Journal*, vol. 22, no. 4, pp. 581–588, 2018.

[19] D. Ma, J. J. Wang, and Z. H. Li, "Effect of particle erosion on mining-induced water inrush hazard of karst collapse pillar," *Environmental Science and Pollution Research*, vol. 26, no. 19, pp. 19719–19728, 2019.

[20] D. T. Snow, "Anisotropie permeability of fractured media," *Water Resources Research*, vol. 5, no. 6, pp. 1273–1289, 1969.

[21] C. Yu and D. Li, "Heterogeneity characteristics of flow and transport fields through rough-walled fractures," *European Journal of Environmental and Civil Engineering*, vol. 22, no. 5, pp. 614–627, 2016.

[22] Y. Ju, Q. G. Zhang, Y. M. Yang, H. P. Xie, F. Gao, and H. J. Wang, "An experimental investigation on the mechanism of fluid flow through single rough fracture of rock," *Science China Technological Sciences*, vol. 56, no. 8, pp. 2070–2080, 2013.

[23] F. Xiong, Q. H. Jiang, Z. Y. Ye, and X. B. Zhang, "Nonlinear flow behavior through rough-walled rock fractures: the effect of contact area," *Computers and Geotechnics*, vol. 102, pp. 179–195, 2018.

[24] Z. Y. Zhang and J. Nemcik, "Fluid flow regimes and nonlinear flow characteristics in deformable rock fractures," *Journal of Hydrology*, vol. 477, pp. 139–151, 2013.

[25] J. Q. Zhou, M. Wang, L. C. Wang, Y. F. Chen, and C. B. Zhou, "Emergence of nonlinear laminar flow in fractures during shear," *Rock Mechanics and Rock Engineering*, vol. 51, no. 11, pp. 3635–3643, 2018.

[26] Y. Chen, W. Liang, H. Lian, J. Yang, and V. P. Nguyen, "Experimental study on the effect of fracture geometric characteristics on the permeability in deformable rough-walled fractures," *International Journal of Rock Mechanics and Mining Sciences*, vol. 98, pp. 121–140, 2017.

[27] Y. D. Chen, H. Lian, W. Liang, J. Yang, V. P. Nguyen, and S. P. A. Bordas, "The influence of fracture geometry variation on non-Darcy flow in fractures under confining stresses," *International Journal of Rock Mechanics and Mining Sciences*, vol. 113, pp. 59–71, 2019.

[28] L. C. Zou, L. Jing, and V. Cvetkovic, "Shear-enhanced nonlinear flow in rough-walled rock fractures," *International Journal of Rock Mechanics and Mining Sciences*, vol. 97, pp. 33–45, 2017.

[29] L. C. Zou, L. Jing, and V. Cvetkovic, "Roughness decomposition and nonlinear fluid flow in a single rock fracture," *International Journal of Rock Mechanics and Mining Sciences*, vol. 75, pp. 102–118, 2015.

[30] B. Li, Y. J. Jiang, T. Koyama, L. Jing, and Y. Tanabashi, "Experimental study of the hydro-mechanical behavior of rock joints using a parallel-plate model containing contact areas and artificial fractures," *International Journal of Rock Mechanics and Mining Sciences*, vol. 45, no. 3, pp. 362–375, 2008.

[31] P. H. Forchheimer, "Wasserbewegung durch boden," *Zeit Ver Deutsch Ing*, vol. 45, pp. 1782–1788, 1901.

[32] L. I. Farfan-Cabrera, E. A. Gallardo-Hernández, and J. Pérez-González, "Compatibility study of common sealing elastomers with a biolubricant (Jatropha oil)," *Tribology International*, vol. 116, pp. 1–8, 2017.

[33] K. T. Gillen, R. Bernstein, and D. K. Derzon, "Evidence of non-arrhenius behaviour from laboratory aging and 24-year field aging of polychloroprene rubber materials," *Polymer Degradation and Stability*, vol. 87, no. 1, pp. 57–67, 2005.

[34] C. Yang, S. L. Shen, D. W. Hou, S. M. Liao, and D. J. Yuan, "Material properties of the seal gasket for shield tunnels: a review," *Construction and Building Materials*, vol. 191, pp. 877–890, 2018.

[35] J. Yuhao, H. Lijun, M. Qingbin, M. Dan, W. Shengyong, and W. Shuai, "Experimental investigation of the mechanical behaviors of grouted crushed coal rocks under uniaxial compression," *Geomechanics and Engineering*, vol. 16, no. 3, pp. 273–284, 2018.

[36] S. G. Fityus, A. Giacomini, and O. Buzzi, "The significance of geology for the morphology of potentially unstable rocks," *Engineering Geology*, vol. 162, pp. 43–52, 2013.

[37] J. F. W. Gale, S. E. Laubach, R. A. Marrett, J. E. Olson, J. Holder, and R. M. Reed, "Predicting and characterizing fractures in dolostone reservoirs: using the link between diagenesis and fracturing," *Geological Society, London, Special Publications*, vol. 235, no. 1, pp. 177–192, 2004.

[38] J. Y. Wu, M. M. Feng, B. Y. Yu, and G. S. Han, "The length of pre-existing fissures effects on the mechanical properties of cracked red sandstone and strength design in engineering," *Ultrasonics*, vol. 82, pp. 188–199, 2018.

[39] H. P. Xie, H. Q. Sun, Y. Ju, and Z. G. Feng, "Study on generation of rock fracture surfaces by using fractal interpolation," *International Journal of Solids and Structures*, vol. 38, no. 32-33, pp. 5765–5787, 2001.

[40] B. B. Mandelbrot, *The Fractal Geometry of Nature*, WH Freeman, New York, NY, USA, 1983.

[41] S. H. Ji, H. B. Lee, I. W. Yeo, and K. K. Lee, "Effect of nonlinear flow on DNAPL migration in a rough-walled fracture," *Water Resources Research*, vol. 44, no. 11, 2008.

[42] C. C. Xia, X. Qian, P. Lin, W. M. Xiao, and Y. Gui, "Experimental investigation of nonlinear flow characteristics of real rock joints under different contact conditions," *Journal of Hydraulic Engineering*, vol. 143, no. 3, 2017.

[43] Q. Yin, G. W. Ma, H. W. Jing et al., "Hydraulic properties of 3d rough-walled fractures during shearing: an experimental study," *Journal of Hydrology*, vol. 555, pp. 169–184, 2017.

[44] M. Wang, Y. F. Chen, G. W. Ma, J. Q. Zhou, and C. B. Zhou, "Influence of surface roughness on nonlinear flow behaviors in 3d self-affine rough fractures: lattice Boltzmann simulations," *Advances in Water Resources*, vol. 96, pp. 373–388, 2016.

[45] R. W. Zimmerman, A. Al-Yaarubi, C. C. Pain, and C. A. Grattoni, "Non-linear regimes of fluid flow in rock fractures," *International Journal of Rock Mechanics and Mining Sciences*, vol. 41, no. 3, pp. 163–169, 2004.

[46] D. Ma, H. Y. Duan, X. B. Li, Z. H. Li, Z. L. Zhou, and T. B. Li, "Effects of seepage-induced erosion on nonlinear hydraulic properties of broken red sandstones," *Tunnelling and Underground Space Technology*, vol. 91, article 102993, 2019.

[47] W. Zhang, B. B. Dai, Z. Liu, and C. Y. Zhou, "A pore-scale numerical model for non-Darcy fluid flow through rough-walled fractures," *Computers and Geotechnics*, vol. 87, pp. 139–148, 2017.

[48] Z. W. Zeng and R. Grigg, "A criterion for non-Darcy flow in porous media," *Transport in Porous Media*, vol. 63, no. 1, pp. 57–69, 2006.

[49] D. Ma, X. Cai, Q. Li, and H. Y. Duan, "In-situ and numerical investigation of groundwater inrush hazard from grouted karst collapse pillar in longwall mining," *Water*, vol. 10, no. 9, article 1187, 2018.

[50] G. Rong, J. Yang, L. Cheng, and C. B. Zhou, "Laboratory investigation of nonlinear flow characteristics in rough fractures during shear process," *Journal of Hydrology*, vol. 541, Part B, pp. 1385–1394, 2016.